LASER INTERFEROMETER GRAVITATIONAL WAVE OBSERVATORY
- LIGO -
CALIFORNIA INSTITUTE OF TECHNOLOGY
MASSACHUSETTS INSTITUTE OF TECHNOLOGY

Technical Note	**LIGO-T1400461-2-**	2014/09/19

Earthquake early warning system for Advanced LIGO

Sebastien Biscans[1], Michael Coughlin[2], Jan Harms[3], Jameson Graef Rollins[4]
[1]*Massachusetts Institute of Technology,* [2]*Harvard University,* [3]*INFN Firenze,* [4]*California Institute of Technology*

California Institute of Technology
LIGO Project, MS 18-34
Pasadena, CA 91125
Phone (626) 395-2129
Fax (626) 304-9834
E-mail: info@ligo.caltech.edu

Massachusetts Institute of Technology
LIGO Project, Room NW22-295
Cambridge, MA 02139
Phone (617) 253-4824
Fax (617) 253-7014
E-mail: info@ligo.mit.edu

LIGO Hanford Observatory
Route 10, Mile Marker 2
Richland, WA 99352
Phone (509) 372-8106
Fax (509) 372-8137
E-mail: info@ligo.caltech.edu

LIGO Livingston Observatory
19100 LIGO Lane
Livingston, LA 70754
Phone (225) 686-3100
Fax (225) 686-7189
E-mail: info@ligo.caltech.edu

http://www.ligo.caltech.edu/

1 Introduction

Detailed studies of earthquake response during S5 and S6 showed that there is about one teleseismic event each week ***FIXME: check number*** producing ground motion at the sites too strong for the control system to be able to maintain lock. In most cases, it was then impossible to lock the interferometer for some hours. A scheme that would suppress disturbances of earthquakes early in the isolation system with the final goal to maintain lock during strong ground motion, even at the price of increased instrumental noise, could potentially lead to substantial increase of the duty cycle. This will likely be of greater importance even in high-power configurations of the advanced detectors, where thermalization of test masses during the locking procedure could potentially increase the time it takes to reach maximal sensitivity.

For this reason, we have created an earthquake early warning client using a real-time event messaging system of the US Geological Survey. The messages contain information about the fault rupture such as location, depth, magnitude. They are received and processed in real time to estimate arrival times, and seismic amplitudes of the various seismic phases at the detector sites. Basic performance evaluations have been carried out already as explained in Section 2, but additional studies carried out over a longer period of time are required to assess more precisely false-dismissal rates. In addition, it is important to investigate how the client can be implemented ***FIXME: Sentence stops here since I have no clue what words to use...***. Finally, further effort needs to be spent on investigating the effect of strong ground motion on the aLIGO control system, and to develop methods for adapting the controls as a means of "riding out the earthquake".

2 Previous investigations

Early earthquake warning (EEW) is a rapidly developing field [1, 2, 3, 4, 5, 6, 7, 8]. The efforts include California systems such as Berkeley's ElarmS and Stanford's Quake-Catcher Network, Japan's Earthquake Early Warning System, and systems in other countries, including Taiwan, Mexico, Turkey, and Romania. All EEW systems seek to rapidly detect and characterize earthquakes shortly after they occur. The goal is to give warning to people before the most severe shaking occurs.

During the last LIGO science run, large amplitude earthquakes from around the world would typically cause the detectors to fall out of lock. Not only were the data around the time of the earthquake not useful for GW detection, but it would also take a significant amount of time for the detectors to return to the locked state. Although there have not yet been detailed effects of this phenomena (which are underway to characterize the effects on the advanced detectors), we can perform a simple back of the envelope calculation here to motivate the study. During the last data collection run, there were 1080 and 1405 science segments for the Hanford and Livingston detectors respectively, corresponding to 87.7 and 67.5 days of science time. Taking the earthquakes with magnitudes greater than 6.0 that occured during that time, loss of interferometer lock occured 54 and 47 times within an hour of the expected surface wave arrivals. These locks had a total downtime of 4.4 and 6.9 days respectively. Although these estimates are likely conservative (loss of lock occurs for a variety of reasons),

they provide an order of magnitude estimate of the potential gains to be made with an early warning system.

We begin by presenting a review of earthquakes and early warning systems. Seismic waves can be split up into two major categories, surface and body waves. Surface waves travel across the surface of the Earth, while body waves travel through the interior. Body waves propagate in three dimensions, radiating spherically from the epicenter of their source. Surface waves instead propagate in two dimensions, which means they decay more slowly with distance than the body waves. Surface waves also tend to have larger particle motion than body waves, which increases the damage they cause. As body waves travel through the Earth, the path of the waves are refracted by variations in the density and shear modulus, which is the ratio of shear stress to the shear strain.

There are two predominant types of body waves, both of which will be important for low-latency earthquake identification. The first are primary waves (P-waves), otherwise known as pressure waves, which are longitudinal, compressional waves. They are the fastest of the wave types, with speeds ranging from 6-13 km/s, and therefore arrive at seismometers first. Low-latency location estimates typically rely on the P-wave arrivals at a number of stations. The second are secondary waves (S-waves), otherwise known as shear waves, which are transverse waves. Shear waves arrive after the P-waves, with speeds ranging from 3-6 km/s. They do not travel through fluids, such as the core, as shear stresses are not supported in fluids. Surface waves come in three different flavors, Rayleigh waves, Love waves, and Stoneley waves. As they all have similar seismic velocities, we will not differentiate between different types of surface waves here. They travel along the surface of the Earth with a velocity lower than those of the body waves. They experience significant dispersion as they travel along the surface, which stretches out their arrival at a given location in time. They also tend to have larger amplitudes than those of body waves. The final type, which does not have significant bearing on the telescopes, are normal modes of the Earth arising from interference from surface waves traveling in opposite directions which generate surface standing waves [9]. Earth's slowest normal-mode oscillation occurs at about 0.3 mHz, and distinct modes can still be identified up to a few millihertz. At higher frequencies, the discrete vibrational spectrum transforms into a quasi-continuous spectrum of seismic vibrations that are increasingly dominated by local sources.

We now briefly describe the process by which earthquakes are identified and what the ground motion due to the events look like. Figure 1 shows example timeseries and a spectrogram at LIGO Hanford for the May 24, 2014 6.9 magnitude Aegean Sea earthquake. After an earthquake occurs, seismometers nearest the epicenter first record the P-wave arrivals. Using a number of arrivals, the latitude and longitude of the event can be determined. Magnitude estimates come later, which measure the total moment release of the earthquake. This is computed by multiplying the distance a fault moved and the force required to move it. Seismometers read out the ground velocity beneath them. Conventional seismometers are simple to convert from raw data to ground velocity, as their response is flat between 0.01 Hz – 1 Hz and relative calibration errors of broadband seismometers between lie well below 0.1 [10].

Given latitude, longitude, and depth information, both P- and S-wave arrivals can be accurately determined. Using the iaspei-tau package [11] wrapped by Obspy [12], travel times

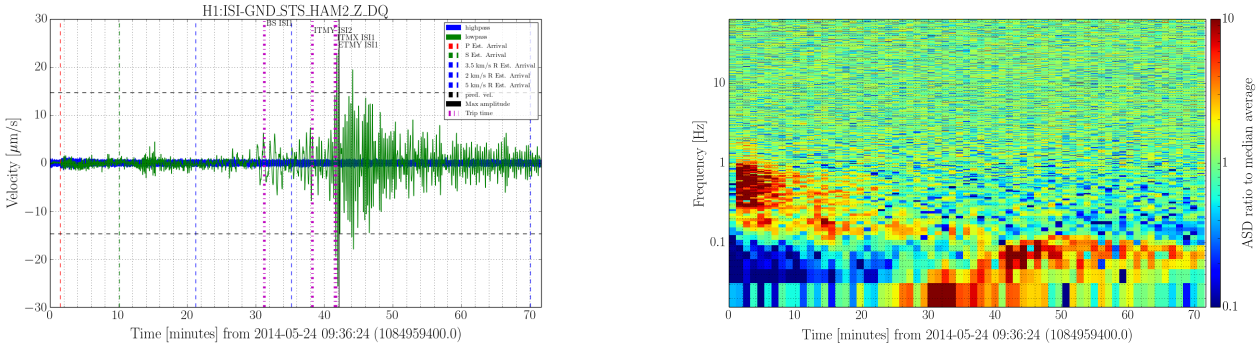

Figure 1: Time-series of ground motion data from recent earthquake. The plot on the left is the ground motion from a seismometer at the LIGO Hanford site located in Washington, USA for the May 24, 2014 6.9 magnitude Aegean Sea earthquake. The P, S, and surface waves all have distinctive arrivals in this case. The surface waves are shown to last tens of minutes. The plot on the right shows a time-frequency spectrogram of the ground motion. The P-wave arrivals have frequency content predominantly between 0.1-1 Hz. The surface wave arrivals instead have frequency content below 0.1 Hz, which leads to the breakdown of the LIGO seismic isolation platform.

for the P (pressure) and S (shear) wave components are calculated for known earthquakes. Approximate arrival times for the surface waves are calculated assuming constant 3.5 km/s speed values. The left of figure 2 shows the time delay between the earthquake and approximate arrival of surface waves for the LIGO Hanford site. In the case of LIGO Hanford, the amount of time between earthquake and surface wave arrival is typically more than 10 minutes long. Location and magnitude estimates for these events are typically generated within a few minutes by USGS and distributed for observatory use through USGS's Product Distribution Layer (PDL), which has been configured to receive all notifications of earthquakes worldwide [13]. This portal will be sufficient for the purposes of current gravitational-wave detectors, which are typically built far from subduction zones (the future KAGRA interferometer at the Kamioka mine in Japan could be an exception to this rule [14]). The right of figure 2 shows the potential warning times provided by the PDL client for the gravitational wave detectors. A majority of the locations allow for more than a minute of time between notification and site arrival.

We have outlined the considerations of an EEW system, and we now turn our attention to the effect of earthquakes on the observatories. To do so, we examine the historical earthquake record and predict the likely ground motion seen. We then use seismic data from on site observations to predict how ground motion will affect the observatories. We have developed an equation attempting to account for physical effects with variable parameters used to fit to the data. Coupling strength of a source at a certain depth to surface Rf waves, dissipation during propagation, geometric amplitude evolution, and frequency dependent scaling of the magnitude into ground displacement were some of the terms used. A few more terms, not physically motivated, were also used to improve the fit. We estimate the amplitude of the surface waves, Rf_{amp}, at the sites using the equation

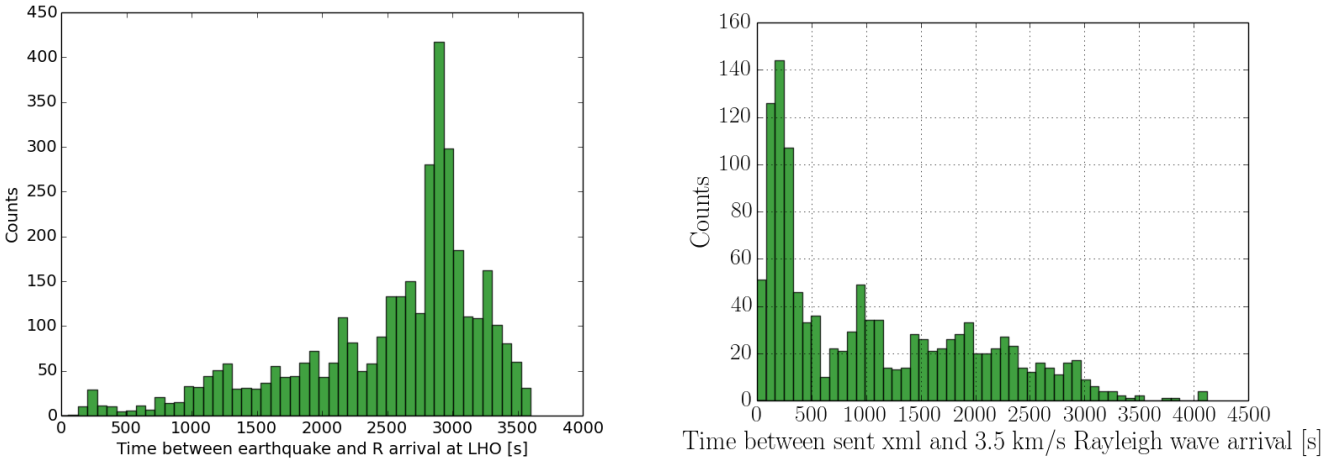

Figure 2: The left plot shows a time delay between the earthquake and approximate arrival of surface waves at the LIGO Hanford site. A majority of the earthquakes are at distances such that their surface waves arrive at the site more than 10 minutes later. The right shows the time delay between the earthquake notification from the PDL client and approximate arrival of surface waves at the LIGO Hanford site. A majority of the locations allow for more than a minute of time between notification and site arrival.

$$Rf_{amp} = 10^{-3} * M * Af * e^{-2*pi*h*fc/cd} * e^{-2*pi*r*fc/ch/Q}/r^{rs} \quad (1)$$

where $fc = 10^{2.3-M/2}$, $Q = \frac{Q0}{fc^{Qs}}$, $Af = \frac{Rf0}{fc^{Rfs}}$, M is the magnitude of the earthquake, d is the distance, h is the depth of the earthquake, c is the speed of the surface-waves, and f_c is the corner frequency. The best fit parameters for the above equation to the measured earthquake arrivals are Rf0 = 0.89256174, Rfs = 1.3588703, Q0 = 4169.7511, Qs = -0.017424297, cd = 254.13458, ch = 10.331297, and rs = 1.0357451. These parameters come from minimizing the difference between the amplitude seen at the interferometer and that predicted by the equation. The regression is shown on the left of Fig. 3. The right of Fig. 3 shows the relative difference between the predicted and actual values. About 94% of events are within a factor of 4, while those that are not are almost exclusively events that are overlap of many events. This occurs often during aftershocks of large earthquakes. As the largest event is the important one, these are unimportant for predictions. Events that produce large surface waves without visible body waves are few. These are more likely to be blasts of some kind.

We now measure the amplitude of the seismic ground motion that creates trips. To do so, we take all known earthquakes above magnitude 5.0 and compute their arrival times. We also determine the platform trips that have occured during these times. We then find the ground motion at the time of these trips. Fig. 4 shows these times. Trips occur during ground velocities greater than about 0.1 μm/s.

We now calculate the function which we can be used to scale the seismic ground motion to the effect on the detector. Due to non-linearities in the coupling of ground motion to these systems, simple linear transfer functions (where the impulse frequency only affects the response frequency) are not representative. We instead compute what we call a Broadband

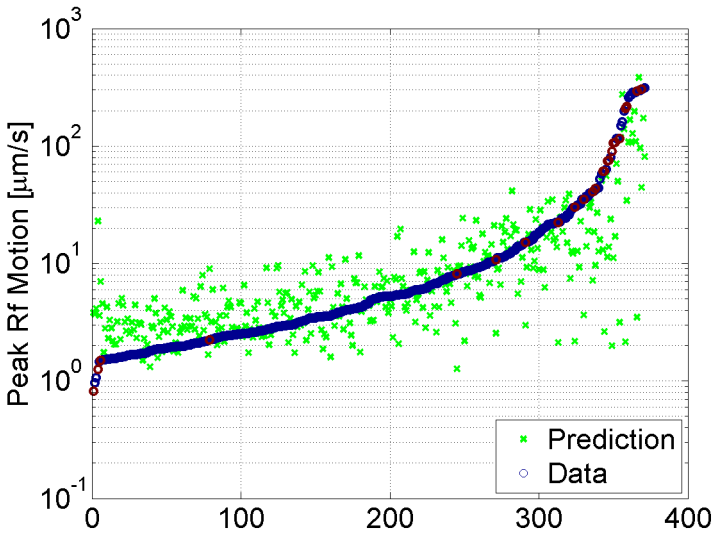

Figure 3: Fit of peak velocities seen at the interferometer to equation 1. The events have been ordered by their measured peak ground velocity (in blue) and the green crosses correspond to the prediction from the equation. About 94% of events are within a factor of 4 of the predicted value.

Motion Response Function (BBMRF), which is the integral of the contribution at any given frequency from all impulse frequencies.

$$H(f) = \int_0^\infty T_f(f')\, df' \tag{2}$$

where $T_f(f')$ is the response to a impulse of frequency f' to f. We use BBMRFs calculated from seismic stations at the observatories during large scale ground motion, one on the ground and another on the instrument platforms. These can be seen in figure 5. LIGO also has significant scaling at earthquake frequencies below 0.1 Hz, particularly at 0.06 and 0.15 Hz. The idea is that we can multiply the spectrum of the earthquakes by this function to find the effective motion of the observatories. We see that the observatories suffer from order of magnitude amplifications of ground motion.

3 Implementation

[15, 16, 17, 18]

4 Controls

References

[1] RM. Allen. Transforming earthquake detection? *Science*, 335:297–298, 2012.

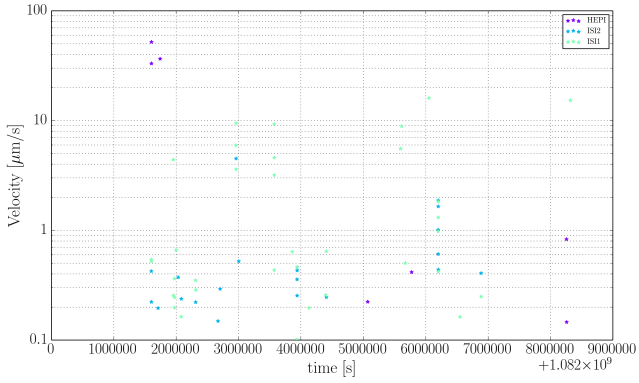

Figure 4: Values of peak ground velocity during earthquakes when the platforms trip. Trips occur during ground velocities greater than about 0.1 μm/s.

[2] Kuyuk, H.S. and RM. Allen. A global approach to provide magnitude estimates for earthquake early warning. *Geophysical Research Letters*, 40, 2013.

[3] Kuyuk, H.S. and RM. Allen. Optimal seismic network density for earthquake early warning: A case study from california. *Seismological Research Letters*, 84(6):946–954, 2013.

[4] Kuyuk, H.S. et al. Designing a network-based earthquake early warning system for california: Elarms-2. *Bulletin of Seismological Society of America*, 104(1), 2014.

[5] Cochran E., Lawrence J., Christensen C., and Chung A. A novel strong-motion seismic network for community participation in earthquake monitoring. *IEEE Inst and Meas*, 12(6):8–15, 2009.

[6] Cochran E., Lawrence J., Christensen C., and Jakka R. The quake-catcher network: Citizen science expanding seismic horizons. *Seismological Research Letters*, 80:26–30, 2009.

[7] M. Bse, R. Allen, H. Brown, G. Gua, M. Fischer, E. Hauksson, T. Heaten, M. Hellweg, M. Liukis, D. Neuhauser, P. Maechling, K. Solanki, M. Vinci, I. Henson, O. Khainovski, S. Kuyuk, M. Carpio, M.-A. Meier, and T. Jordan. Cisn shakealert: An earthquake early warning demonstration system for california. In Friedemann Wenzel and Jochen Zschau, editors, *Early Warning for Geological Disasters*, Advanced Technologies in Earth Sciences, pages 49–69. Springer Berlin Heidelberg, 2014.

[8] Mitsuyuki Hoshiba, Osamu Kamigaichi, Makoto Saito, Shin'ya Tsukada, and Nobuo Hamada. Earthquake early warning starts nationwide in japan. *Eos, Transactions American Geophysical Union*, 89(8):73–74, 2008.

[9] Montagner J and Roult G. Normal modes of the earth. *Journal of Physics: Conference Series*, 118(1):012004, 2008.

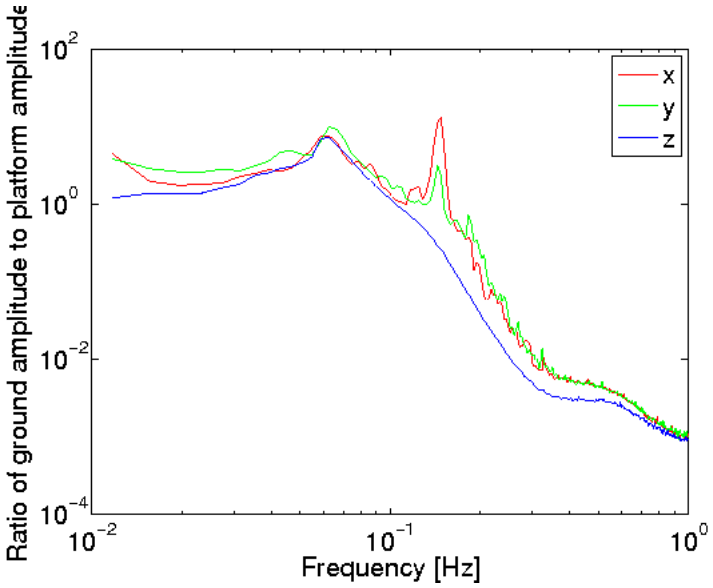

Figure 5: Affect of strong ground motion on LIGO Hanford. The plot shows the Broadband Motion Response Function for LIGO. LIGO also has significant scaling at earthquake frequencies below 0.1 Hz, particularly at 0.06 and 0.15 Hz.

[10] F. L. Vernon and D. Harvey and J. A. Eakins and R. W. Busby and L. Astiz and R. L. Newman and J. Reyes. Calibration Response of the NSF Earthscope USArray Transportable Array. *calibration of USArray*, 2009.

[11] Snoke J.A. Traveltime tables for iasp91 and ak135. *Seismological Research Letters*, 80(2):260–262, 2009.

[12] Moritz Beyreuther, Robert Barsch, Lion Krischer, Tobias Megies, Yannik Behr and Joachim Wassermann. Obspy: A python toolbox for seismology. *Seismological Research Letters*, 81(3):530–533, 2010.

[13] United States Geological Survey. Product distribution user guide. *ehppdl1.cr.usgs.gov*, 2012.

[14] Yoichi Aso, Yuta Michimura, Kentaro Somiya, Masaki Ando, Osamu Miyakawa, Takanori Sekiguchi, Daisuke Tatsumi, and Hiroaki Yamamoto. Interferometer design of the kagra gravitational wave detector. *Phys. Rev. D*, 88:043007, Aug 2013.

[15] J. Rollins. Advanced LIGO Automation Requirements. *LIGO DCC*, T1300884, 2013.

[16] J. Rollins. Advanced LIGO Guardian Overview and User Manual. *LIGO DCC*, G1400016, 2014.

[17] S. Waldman and M. Evans. Advanced LIGO System Guardian. *LIGO DCC*, T1000131, 2010.

[18] R. Bork. RCG V2.9 - Loading and Monitoring of BURT settings by front end controls computers. *LIGO DCC*, G1400742, 2014.